Semnan University

Progress in Physics of Applied Materials

Journal homepage: https://ppam.semnan.ac.ir/

Preparation of TiO_2 nanostructures and its plasma coating in the Dye-Sensitized Solar Cell

Zeynab Kiamehr [a*]

[a] *Department of Physics, Tafresh University, Tafresh, Iran*

ARTICLE INFO

Article history:

Received: 15 September 2024
Revised: 9 October 2024
Accepted: 16 October 2024

Keywords:

Plasma treatment;
Dye-Sensitized Solar Cell;
TiO_2 nanostructures;
Thin film solar cell;
Efficiency.

ABSTRACT

In this research, TiO_2 nanostructures were prepared using the hydrothermal method. The aerosol was regenerated from the precursor solution droplets by entering the non-thermal plasma and TiO_2 nanostructures were deposited on the surface of the substrate. XRD and SEM analyses have been used to investigate nanostructure morphology. Dye-sensitized solar cells were fabricated using TiO_2 nanostructures as a photoanode. The results showed that the surface prepared with TiO_2 nanostructures by the hydrothermal method has a higher specific surface area, more pigment absorption, and short circuit current density than the unmodified surface. In addition, the TiO^2 photoanode-based pigment solar cell using the hydrothermal method showed a short circuit current density of 21.67 mA/cm^2, an open-circuit voltage of 0.67 V, and a photon-to-electricity conversion efficiency of 5.62%, which is about 17% more than the yield obtained. This comes from a solar cell without plasma modification with an efficiency of 5.11%. The increase in efficiency can be attributed to the increase in electrical conductivity in the photoanode, the tight connection of the conductive surface of the anode with the pigment molecules, and the greater contact surface of the photoanode with the electrolyte.

1. Introduction

Porous photoanodes in Dye-Sensitized Solar cells are semiconducting metal oxides with a thickness of less than 20 microns, such as TiO_2, ZnO, SnO_2, etc. Pigment molecules are placed on metal oxide nanoparticles to absorb sunlight and inject electrons into the photoanode structure [1]. The higher the specific surface area of metal oxide nanoparticles in the photoanode, the more pigment molecules are placed in the structure, and as a result, more electrons are produced in the cell. This phenomenon causes an increase in the production flow and as a result, increases the efficiency [2]. There are many chemical methods to increase the specific surface of metal oxide nanoparticles, which have their problems. Titanium dioxide (TiO_2) has three crystal forms including anatase, rutile, and brookite. In terms of thermodynamics, rutile is the most stable TiO_2 phase at normal pressure, and the other two phases are semi-stable phases of this system. The basic crystal units in all three phases are $TiO6$ octahedral [3]. The difference between these three phases is in the arrangement of these octahedra. These structures are related to TiO_2 masses. Due to the very high surface-to-volume ratio of TiO_2 nanoparticles, the surface arrangement may be completely different from the mass. In recent years, the synthesis of ceramic nanoparticles has received a lot of attention due to their optical and electronic properties and better condensability [4]. Meanwhile, titanium dioxide nanoparticles (TiO_2) have shown good electrical, optical, and photocatalytic properties. The application and efficiency of TiO_2 are strongly influenced by the crystal structure, shape, and size of its particles. Therefore, many efforts have been made to produce TiO_2 nanoparticles with controlled size, shape, and porosity for use in thin layers, ceramics, composites, and catalysts [4]. TiO_2 is a material that is used in various fields such as paints, plastics, cosmetics, inks, papers, and sensors. The increase in the use of TiO_2 nanoparticles in catalytic, photocatalytic, and sensor fields has intensified the need to use precise equipment for their synthesis. In many cases, TiO_2 is produced using the sulfate or chloride Anions, but the produced particles are relatively coarse (in the micron range) and have a low degree of purity. With the increasing need to use nanoparticles, TiO_2, much research has been done in this field [5]. Of course, the expensiveness of TiO_2 nanoparticles, which is caused by the complex processes of

* **Corresponding author.**
E-mail address: z.kiamehr@tafreshu.ac.ir

Cite this article as:
Kiamehr, Z., 2025. Preparation of TiO_2 nanostructures and its plasma coating in the Dye-Sensitized Solar Cell. *Progress in Physics of Applied Materials*, *5*(1), pp.11-16. DOI: 10.22075/ppam.2024.35331.1117

their synthesis, has limited the use of these materials to some extent. To solve this problem, simple processes should be developed that reduce the price of nanoparticles by increasing production efficiency [6].

So far, several methods have been used for the synthesis of TiO_2 nanoparticles, among which the hydrothermal method can be mentioned. The hydrothermal method is used only for the synthesis of simple and mixed oxide powders with controlled morphology, at a relatively low temperature (100-350ºC). Generally, nanomaterials synthesized by hydrothermal methods are produced under high steam pressure conditions. They can lead to product production with minimal loss of raw materials. In hydrothermal synthesis, the nanomaterials to be synthesized can be well controlled through the liquid volume. Since many parameters are involved in the hydrothermal process, researchers have used different composite models in different hydrothermal methods for the synthesis of TiO_2 nanoparticles [6]. Yang et.al., used pressure in the heating step and reduced the working temperature. In this method, TiO_2 deposits were prepared by adding dropwise 0.5 M titanium butoxide isopropanol solution to deionized water. The white precipitates were washed with deionized water and with the help of centrifugal force, and after neutralization by HNO_3, they were dried for 1 hour at 70ºC. It was observed that depending on the different amounts of neutralizing agent, prepared nanoparticles have different shapes and average size between 15-50nm and they are completely in the form of anatase or rutile phase [7].

In recent decades, plasma methods for the production and deposition of nanomaterials have received more attention due to the presence of active species such as ions, electrons, radicals, and energetic photons, the plasma environment has the necessary conditions [8]. The plasma environment provides the advancement of chemical and physical reactions to the deposition of nanomaterials at low temperatures. Plasma electrons play an effective role in reducing metal precursors to produce desired nanomaterials. In recent research, it was found for liquid phase precursors that plasma electrons can penetrate in contact with the liquid surface and directly reduce dissolved metal ions to finally produce desirable nanomaterials [9]. Plasma deposition methods have many advantages over other conventional methods. In these methods, the number of steps in the deposition process is small and these processes proceed at low temperatures. This allows the use of temperature-sensitive substrates. Among other advantages of plasma methods, we can mention the reduction of production cost, electricity consumption, and waste of raw materials [10]. It should also be noted that plasma deposition methods do not require initial modification of the substrate surface and final curing of the created layer [11]. Traditional plasma requires a vacuum to deposit nanomaterials, and in recent years, non-thermal plasma jets have been proposed to deposit copper oxide, titanium oxide, tin oxide, reduced graphene oxide, and silver nanostructures [11]. Hong and co-workers produced and deposited gold nanoparticles directly from chloroauric acid ($HAuCl_4$) solution, which they used for surface Raman scattering [12].

In the radio frequency thermal plasma method, the precursor used is vaporized by radio frequency thermal plasma and by performing a chemical reaction, nanoparticles are prepared from the vapor phase. This type of plasma can be used to synthesize nanoparticles from many minerals. The very high speed of cooling and the high concentration of reactive radicals in the plasma environment have made this method a unique process for the synthesis of nanoparticles [10]. Lee et al. used this method to synthesize TiO_2 nanoparticles from an organic precursor. The XRD results showed that the nanoparticles are formed between 71-78% by weight of the anatase phase and their average size is about 50 nm. Oh et.al also used this method to synthesize TiO_2 nanoparticles from an inorganic precursor. The XRD patterns showed that the nanoparticles have both anatase and rutile phases with an average size of 50 nm [13].

In this work, TiO_2 nanostructures are produced and deposited directly with the help of a non-thermal plasma jet. The precursor solution is injected into the plasma as an aerosol. Finally, the properties of the plasma-coated surface and its performance are investigated by different analyses and compared with the sample without coating.

2. Experimental Details

2.1 Preparation of TiO_2 nanostructure

In this research, the microwave hydrothermal method was used for the synthesis of TiO_2 nanostructures [14]. In this method, TiCL4 was diluted with distilled ice water to form TiO_2 solution (0.2M). In the obtained solution, the specific amount of urea (the ratio of Ti to Urea is 1:5) was dissolved and the resulting mixture was placed in transparent containers to provide the possibility of microwave radiation. After microwave irradiation, the solid product was filtered and washed twice with distilled water. Then the crystalline powder was deposited, filtered, and dried in a dryer. Very high production speed and very fast heating up to operating temperature are among the advantages of this method.

2.2 Construction of photoanode

To make the photoanode, first, the FTO conductive glasses were subjected to ultrasonication with distilled water, acetone, isopropanol, and ethanol each for 20 minutes. To prevent the recombination of electrons and holes with each other, the substrates were placed in 40 mM $TiCl_4$ aqueous solution at 70 degrees for 30 minutes.

Fig. 1 shows the non-thermal plasma jet for deposition. This jet works with a dielectric barrier discharge configuration that has two copper electrodes wrapped on the surface of the quartz tube at a distance of 1 cm from each other. This quartz tube with an inner diameter of 2 mm and an outer diameter of 4 mm is used as a dielectric in this plasma jet. Plasma gas flows inside this quartz tube

along with aerosol carrier gas. To produce plasma, these electrodes are connected to a high-voltage power supply, between 5 to 10 kV and a working frequency of 20 kHz, and the voltage applied to the plasma is measured by a high-voltage probe and an oscilloscope [15].

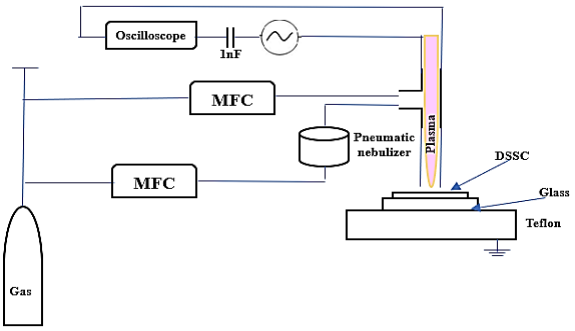

Fig. 1. Schematic view of the plasma device used in this research

In this system, argon gas is used as plasma gas and aerosol carrier gas. The plasma gas flow rate is 2 SLPM and the carrier gas is 0.5 SLPM. After passing through the pneumatic nebulizer, the carrier gas creates an aerosol from drops of TiO_2 which is added to the plasma gas and flows along with it into the plasma jet quartz tube. After passing through the gap between two electrodes, this gas becomes a plasma and is radiated to the surface of the glass substrate. The distance between the substrate and the plasma nozzle is 3 mm. The surface of the glass substrates is completely cleaned and free of any contamination with acetone, ethanol, and deionized water before the coating. The prepared solution is converted into small droplets with sizes of 2 to 10 micrometers by a nebulizer. These tiny droplets are suspended in the plasma for a very short time. Active plasma species, especially electrons, hit the surface of the droplets suspended in the plasma, and penetrate the surface of the droplets.

The creation of TiO_2 nanostructures in this research includes two steps. In the first step, powdery TiO_2 crystal structures were obtained through microwave hydrothermal method and dissolved in water. In the second step, using a nebulizer, the solution containing TiO_2 is broken into smaller particles to be uniformly distributed as suspended droplets in the Ar plasma gas. Finally, the studied surface was coated using a cold plasma jet. Together, these two gases (the gas containing TiO_2 nanostructures and the Ar gas) provided the necessary combined plasma for layering. After coating, the samples were dried in an oven at 120 degrees for 30 minutes. In the next step, the layers were placed in 0.5 mM of N719 solution for 24 hours.

2.3 The cathode and the cell fabrication

To introduce the electrolyte-containing $\mathbf{I^-/I_3^-}$, using a miniature drill, a single small hole was created on the FTO substrates, and the substrates were washed completely.

Then a drop of 10 mM H2PtCl6 solution was dripped on the FTO substrates and after drying, they were heated at 450 degrees for 30 minutes. The photoanode and cathode prepared in the previous steps were glued together. The electrolyte containing, I^- / I^{3-} entered the cell by creating a vacuum from the side of the hole installed on the counter electrode. Finally, using glass and glue, the hole was completely covered.

3. Results and Discussion

Fig. 2 shows the images obtained from SEM and TEM analyses. Using DigiMizer software, the average size of seeds, and using Origin software and the normal log function, standard deviation, and a column graph of seed abundance in different intervals have been drawn [16]. After obtaining the grain size randomly by the DigiMizer software, the data were fitted using the Origin software with the log-normal function, and the average grain size and standard deviation were obtained using the following formulas.

$$F(D) = (2\pi\sigma_D)^{-1/2}\, e^{\left(\frac{Ln(D/D_0)^2}{2\sigma^2}\right)} \quad (1)$$

$$< D >= D_0 e^{(\sigma^2/2)} \quad (2)$$

$$\sigma_D =< D > \sqrt{e^{\sigma^2} - 1} \quad (3)$$

D_0 and σ are constant parameters, D is the average particle size and σ_D is the standard deviation (Fig. 2).

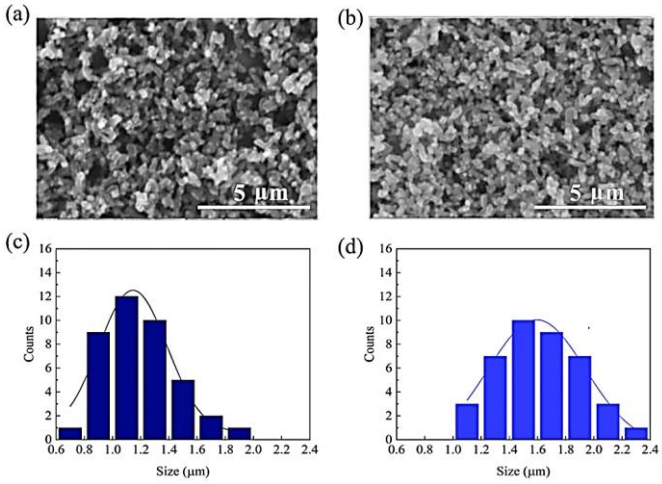

Fig. 2. The SEM analysis results of the unmodified and plasma-modified FTO

D_0, the standard deviation and average diameter of the particles on the surface for the unmodified sample without plasma coating (Fig. 2c) are 71.45, 0.42, and 87.63 nm, respectively, and for the sample modified by plasma by TiO_2 nanostructures (Fig. 2d). 103.76, 0.39, and 121.27 nm are estimated. Fig. 3 shows the SEM image of TiO_2 powder obtained by the microwave hydrothermal method, which shows its crystallinity phase before it is dissolved in water and placed in the nebulizer.

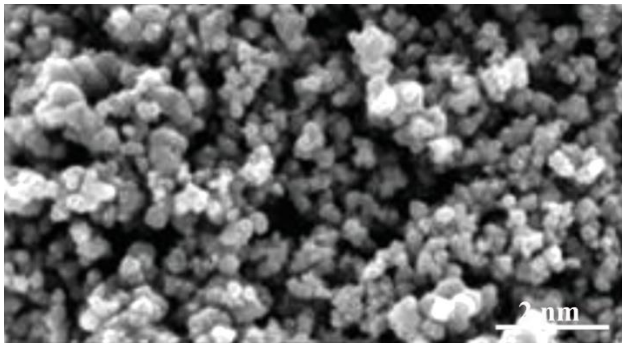

Fig. 3. The SEM analysis results of the TiO_2 powder in this research.

Fig. 4 shows the X-ray diffraction pattern for the unmodified and the plasma-modified sample by TiO_2 nanostructures. It can be seen that the diffraction pattern has peaks that represent planes (101), (103), (004), (112), (002), (105), (211), (204), (116), (220), (215), and (224). These plates confirm the TiO_2 crystallinity phase. Also, the diffraction pattern for the modified surface shows higher peaks, which are related to TiO_2, while these peaks are also present in the unmodified sample surface with lower intensity [17].

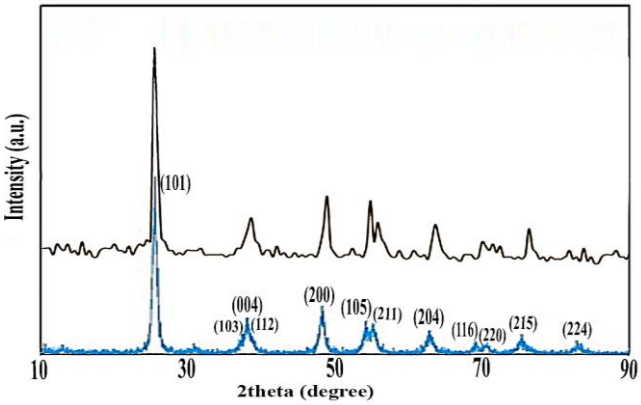

Fig. 4. The XRD analysis results of the unmodified (down) and plasma-modified DSSC (up)

The optical spectroscopy method was used to investigate the specific surface of semiconductors. The photoanode layers were placed in 0.1M sodium hydroxide (NaOH) solution with ethanol solvent for one hour to separate the N719 pigment from the surface of the nanostructures [18]. The obtained pink solution was poured into a quartz cell and its absorption spectrum was measured (Fig. 5). Based on pigment absorption and solution concentration measurement using Beer-Lambert law ($A = \varepsilon bc$), the amount of pigment loaded in the photoanode structure modified with plasma containing TiO_2 nanostructures was estimated to be 9.78 mol/cm^2 and 8.01 mol/cm^2 for the unmodified surface. In the Beer-Lambert law, A is the absorption coefficient, ε is the molar absorption coefficient of pigment N719, c is the concentration, and b is the length of the part of the solution that is placed in the light path.

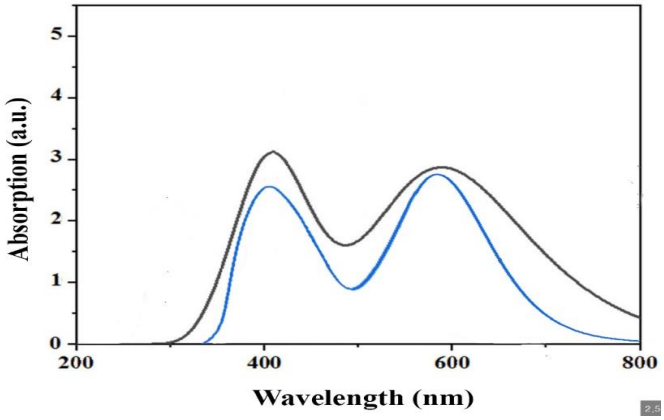

Fig. 5. The absorption spectrum of pigment N 719 in 0.1 M NaOH solution with ethanol solvent of the unmodified (down) and plasma-modified DSSC (up)

Fig. 6 shows the current-voltage curve and the parameters obtained from the current-voltage curve for solar cells in two states modified with plasma containing TiO_2 nanostructures and without modification. The short circuit current density (J_{sc}) for plasma-modified cells is increased compared to unmodified cells. The increase in specific surface area in plasma-modified semiconductors has absorbed more dyes and more photons have been converted into excitons. This factor has caused an increase in J_{sc} in solar cells modified by plasma-containing TiO_2 nanostructures [19, 20].

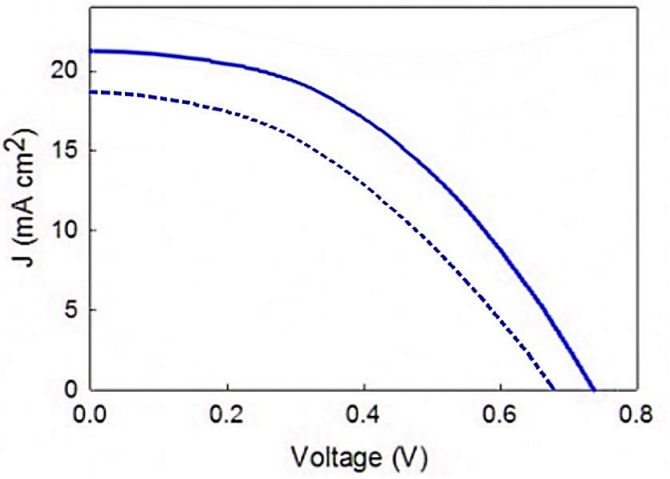

Fig. 6. The current-voltage curve of the solar cell of the unmodified sample (down) and plasma-modified sample by TiO_2 nanostructures (up)

Table 1. Parameters obtained from the current-voltage diagram

Sample	V_{oc} (volt)	Fill factor	Jsc (mA/cm^2)	Efficiency (%)
FTO without plasma treatment	0.65	0.28	21.67	5.11
FTO with plasma treatment by TiO_2 nanostructures	0.67	0.28	19.16	5.62

Open circuit voltage (V_{oc}) and fill factor (FF) did not show significant changes for both samples. The best efficiency was obtained for solar cells modified with plasma-containing TiO_2 nanostructures.

Electrochemical impedance spectroscopy (EIS) analysis was performed on cells based on different photoanodes [21]. Fig. 7 shows the Nyquist diagram of cells under exposure conditions. In each Nyquist diagram, two semicircles are observed. R_{ct1} and CPE_1 (constant phase element) correspond to the charge transfer resistance and capacitance at the electrolyte/counter electrode boundary (small semicircle), R_{ct2} and CPE_2 correspond to the resistance Charge transfer and capacitance at the electrolyte/photoanode interface (large semicircle) and R_s are resistances due to junctions. Electrochemical parameters are obtained from impedance spectrum fitting. R_{ct2} was 18.3 Ω for the unmodified cell and 14.2 Ω for the plasma-modified cell containing TiO_2 nanostructures. It is known that the reduction of the resistance at the boundary between the electrolyte/photoanode has increased the ion transfer rate and led to an increase in the current in the cell. The results of this analysis confirm the data obtained from the current-voltage characteristic curve well.

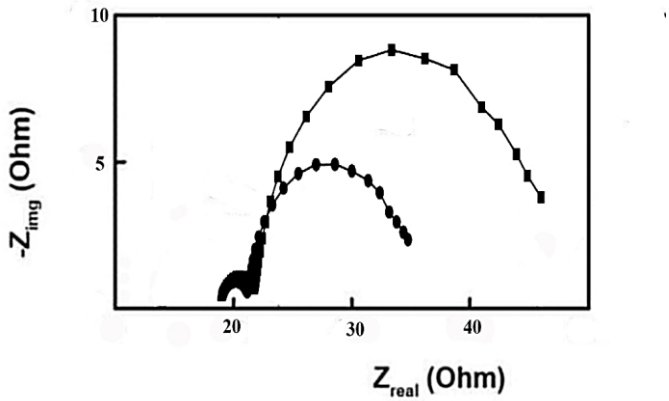

Fig. 7. Nyquist diagram (EIS) for DSSC of the unmodified sample (down) and plasma-modified sample by TiO_2 nanostructures (up)

4. Conclusions

In this research, the microwave hydrothermal method was used to prepare TiO_2 nanostructures for use in the plasma coating machine. After modifying the surface of the DSSC plasma brush, its performance was investigated with the unmodified sample. For comparison, coated TiO_2 nanostructures were used as anodes in dye-sensitized solar cells. DSSC surface modification by the plasma method led to the absorption of more pigment molecules and an increase in the closed-circuit current in the cells. Plasma modification by TiO_2 nanostructures strengthened the connections between the semiconductors of these nanostructures and pigment molecules. In addition, the presence of these nanostructures on the surface of the DSSC increased the contact surface between the electrolyte and the anode and thus improved the performance of the photovoltaic cell. The results of the impedance spectrum also confirmed the data obtained from the current-voltage characteristic curve.

Conflicts of Interest

The author declares that there is no conflict of interest regarding the publication of this article.

References

[1] Salunkhe, R.R., Kaneti, Y.V. and Yamauchi, Y., 2017. Metal–organic framework-derived nanoporous metal oxides toward supercapacitor applications: progress and prospects. *ACS nano*, *11*(6), pp.5293-5308.

[2] Denizalti, S., Ali, A.K., Ela, Ç., Ekmekci, M. and Erten-Ela, S., 2018. Dye-sensitized solar cells using ionic liquids as redox mediator. *Chemical Physics Letters*, *691*, pp.373-378.

[3] Yang, M., Dong, B., Yang, X., Xiang, W., Ye, Z., Wang, E., Wan, L., Zhao, L., Wang, S., 2017. TiO_2 nanoparticle/nanofiber-ZnO photoanode for the enhancement of the efficiency of dye-sensitized solar cells. RSC Advances, 7, p.41738-41744.

[4] Arof, A.K., Noor, I.M., Buraidah, M.H., Bandara, T.M.W.J., Careem, M.A., Albinsson, I. and Mellander, B.E., 2017. Polyacrylonitrile gel polymer electrolyte based dye sensitized solar cells for a prototype solar panel. *Electrochimica Acta*, *251*, pp.223-234.

[5] Liu, R., Qiang, L.S., Yang, W.D. and Liu, H.Y., 2013. Enhanced conversion efficiency of dye-sensitized solar cells using Sm2O3–modified TiO_2 nanotubes. *Journal of power sources*, *223*, pp.254-258.

[6] Jung, H.G., Kang, Y.S. and Sun, Y.K., 2010. Anatase TiO_2 spheres with high surface area and mesoporous structure via a hydrothermal process for dye-sensitized solar cells. *Electrochimica Acta*, *55*(15), pp.4637-4641.

[7] Yang, J., Mei, S. and Ferreira, J.M.F., 2001. Hydrothermal synthesis of TiO_2 nanopowders from tetraalkylammonium hydroxide peptized sols. *Materials Science and Engineering: C*, *15*(1-2), pp.183-185.

[8] Gandhiraman, R.P., Jayan, V., Han, J.W., Chen, B., Koehne, J.E. and Meyyappan, M., 2014. Plasma jet printing of electronic materials on flexible and nonconformal objects. *ACS applied materials & interfaces*, *6*(23), pp.20860-20867.

[9] Gandhiraman, R.P., Singh, E., Diaz-Cartagena, D.C., Nordlund, D., Koehne, J. and Meyyappan, M., 2016. Plasma jet printing for flexible substrates. *Applied Physics Letters*, *108*(12).

[10] Tsumaki, M., Nitta, K., Jeon, S., Terashima, K. and Ito, T., 2018. Development of plasma-assisted inkjet printing and demonstration for direct printing of conductive silver line. *Journal of Physics D: Applied Physics*, *51*(30), p.30LT01.

[11] Dey, A., Lopez, A., Filipič, G., Jayan, A., Nordlund, D., Koehne, J., Krishnamurthy, S., Gandhiraman, R.P. and Meyyappan, M., 2019. Plasma jet based in situ reduction of copper oxide in direct write printing. *Journal of Vacuum Science & Technology B*, *37*(3).

[12] Dey, A., Krishnamurthy, S., Bowen, J., Nordlund, D., Meyyappan, M., 2018. Plasma Jet Printing and in Situ

Reduction of Highly Acidic Graphene Oxide. ACS nano, 12, p.5473-81.
[13] Ramamurti, R., Gandhiraman, R.P., Lopez, A., Doshi, P., Nordlund, D., Kim, B. and Meyyappan, M., 2020. Atmospheric pressure plasma printing of nanomaterials for IoT applications. *IEEE Open Journal of Nanotechnology*, *1*, pp.47-56.
[14] Bregadiolli, B.A., Fernandes, S.L. and Graeff, C.F.D.O., 2017. Easy and fast preparation of TiO_2-based nanostructures using microwave assisted hydrothermal synthesis. *Materials Research*, *20*(4), pp.912-919.
[15] Lou, B.S., Lai, C.H., Chu, T.P., Hsieh, J.H., Chen, C.M., Su, Y.M., Hou, C.W., Chou, P.Y. and Lee, J.W., 2019. Parameters affecting the antimicrobial properties of cold atmospheric plasma jet. *Journal of Clinical Medicine*, *8*(11), p.1930.
[16] Liu, B.T. and Liou, J.Y., 2018. High efficiency of dye-sensitized solar cells with two-layer mesoporous photoanodes fabricated in a low temperature process. *Electrochimica Acta*, *261*, pp.421-427.
[17] Xu, L., Xu, J., Hu, H., Cui, C., Ding, Z., Yan, Y., Lin, P. and Wang, P., 2019. Hierarchical submicroflowers assembled from ultrathin anatase TiO_2 nanosheets as light scattering centers in TiO_2 photoanodes for dye-sensitized solar cells. *Journal of Alloys and Compounds*, *776*, pp.1002-1008.
[18] Zhang, L., Cole, J.M., 2015. Anchoring Groups for DyeSensitized Solar Cells. ACS Applied Materials and Interfaces, 7, p.3427-3455.
[19] Mozaffari, S. and Nateghi, M.R., 2014. Effects of multi anchoring groups of catecholamine polymer dyes on the electrical characteristics of metal free dye-sensitized solar cells: A comparison study. *Solar energy*, *106*, pp.63-71.
[20] Mozaffari, S., Dehghan, M., Borhanizarandi, M. and Nateghi, M.R., 2014. Effect of single-wall carbon nanotubes on the properties of polymeric gel electrolyte dye-sensitized solar cells. *Journal of Solid State Electrochemistry*, *18*, pp.655-663.
[21] Lim, S.J., Kang, Y.S. and Kim, D.W., 2011. Dye-sensitized solar cells with quasi-solid-state cross-linked polymer electrolytes containing aluminum oxide. *Electrochimica Acta*, *56*(5), pp.2031-2035.